JOURNAL OF AIRCRAFT
Vol. 44, No. 3, May–June 2007

Fuzzy-Logic-Based Health Monitoring and Residual-Life Prediction for Composite Helicopter Rotor

Prashant M. Pawar* and Ranjan Ganguli†
Indian Institute of Science, Bangalore 560012, India

DOI: 10.2514/1.26495

A health-monitoring and life-estimation strategy for composite rotor blades is developed in this work. The cross-sectional stiffness reduction obtained by physics-based models is expressed as a function of the life of the structure using a recent phenomenological damage model. This stiffness reduction is further used to study the behavior of measurable system parameters such as blade deflections, loads, and strains of a composite rotor blade in static analysis and forward flight. The simulated measurements are obtained using an aeroelastic analysis of the composite rotor blade based on the finite element in space and time with physics-based damage modes that are then linked to the life consumption of the blade. The model-based measurements are contaminated with noise to simulate real data. Genetic fuzzy systems are developed for global online prediction of physical damage and life consumption using displacement- and force-based measurement deviations between damaged and undamaged conditions. Furthermore, local online prediction of physical damage and life consumption is done using strains measured along the blade length. It is observed that the life consumption in the matrix-cracking zone is about 12–15% and life consumption in debonding/delamination zone is about 45–55% of the total life of the blade. It is also observed that the success rate of the genetic fuzzy systems depends upon the number of measurements, type of measurements and training, and the testing noise level. The genetic fuzzy systems work quite well with noisy data and are recommended for online structural health monitoring of composite helicopter rotor blades.

Introduction

AN INTEREST in developing health- and usage-monitoring systems (HUMS) for helicopter rotors has grown markedly in recent years [1], due to the high levels of unsteady airloads experienced by the main rotor [2–4] that can lead to structural-damage accumulation. However, most of the existing rotor HUMS rely on rotor track-and-balance (RTB) techniques for detecting rotor blade mistracking and do not isolate the type of damage [5–8]. Most research on rotor health monitoring has addressed isotropic blades [9–12]. However, the damage mechanics of a composite rotor are quite different [13–16]. Furthermore, the rotor operates in a noisy environment, which complicates the development of damage-detection algorithms. Therefore, the current need of rotor HUMS is the development of an advanced structural-health-monitoring (SHM) system for the composite rotor blades.

In general, SHM systems are developed based on the study of the effect of different measurable properties of the rotor system that are due to the various modes of damages in the rotor blade. Modern rotor blades are typically made of composite materials. However, very limited work has been done on the modeling of damage in the composite rotor system. Several researchers have investigated the modeling of a damaged helicopter rotor, assuming isotropic structural properties [9,11,17]. Some works considered crack models based on a fracture mechanics approach [18], but these have also been limited to isotropic materials. A first step addressing damage modeling in composite rotor blades was taken by Lakshmanan and Pines [19], who modeled damage in the form of a transverse crack, which extends across the entire width of the flexbeam of a bearingless rotor. However, there is a need for detailed modeling of the damage modes in a composite rotor blade. A beginning in this direction was made by Pawar and Ganguli [13], who modeled matrix cracking in the helicopter rotor blade with cross-ply laminates and studied its behavior in forward flight. Pawar and Ganguli [14] further modeled the matrix cracking in generalized lay-up, box, and airfoil-section beams and studied their static behavior. They also studied [15] the effect of more severe damage modes, such as debonding/delamination and fiber breakage due to matrix cracking, for a static condition [15] and for forward flight [16].

In general, the first failure mode in the composite materials is dominated by matrix cracking. Matrix cracking initiates more severe damage modes such as debonding/delamination and fiber breakage. Therefore, the effects of matrix cracking must be studied carefully. When the matrix-cracking effect starts saturating, a local delamination can initiate from the matrix-crack tips. Even though the effects of delamination are not very severe, it may lead to the dangerous and final damage mechanism of fiber breakage. As a result of matrix-cracking and debonding/delamination damage modes in composite materials, the matrix part of composite materials becomes weak and a proper transfer of the shear loads at the broken fibers may not take place. A detailed literature survey of all of these key damage modes in composite materials is covered in the author's previous papers [15,16].

Most of the SHM systems for rotor blades are developed to predict physics-based damages. Though such works are useful in providing physical insight, what is needed for prognostics is an estimate of life consumption of the blade. Fatigue-damage growth is an important aspect of the evolution of damage in the helicopter rotor blades. To develop the SHM system for predicting the life of composite rotor blades, an analysis of the measurable system behavior of the composite rotor blade due to life consumption of the structure is needed. This allows the use of the system measurements as virtual sensors for the blade life. Generally, the decay in structural properties of composite materials is modeled using phenomenological models for fatigue analysis of the structure [20]. Although the fatigue of homogenous materials is well understood, the analysis of fatigue in composites is difficult, because the material properties of the constituents of composites are quite different and there are multiple failure modes.

Experiments have shown that the variation in the modulus of elasticity due to damage growth in composite materials shows three

Received 12 July 2006; revision received 17 January 2007; accepted for publication 6 February 2007.

*Research Student, Department of Aerospace Engineering; pawar@aero.iisc.ernet.in.

†Associate Professor, Department of Aerospace Engineering; ganguli@aero.iisc.ernet.in. Senior Member AIAA.

different stages [21]. Stage 1 undergoes a rapid stiffness reduction that is mostly due to the development of transverse matrix cracks. Stage 2 damage growth is dominated by delamination and occurs in an almost linear fashion with respect to cycles and accounts for the high fatigue life of composites. Stage 3 shows rapid stiffness degradation purely due to local damage progression and the initial fiber fractures leading to strand failures. Early damage models included a linear damage accumulation model by Nicholas and Russ [22]. Other nonlinear damage accumulation functions have also been used by Subramanian et al. [23] and Halverson et al. [24]. These early models could not effectively capture all three damage stages. For example, the model proposed by Subramanian et al. explains the fast damage growth during the early loading cycles in stage 1, but does not properly describe the rapid damage growth in stage 3. Halverson et al. models stage 3 quite well, but not stage 1. Mao and Mahadevan [25] recently proposed a nonlinear model to capture the unique characteristics of damage evolution in composite materials subject to fatigue loading. Parameters of the proposed model are obtained using experimental data. With the obtained parameters, the fatigue damage can be evaluated at any time. The numerical examples show that the proposed damage function can model the experimental results very well. Fatigue-damage indices during the service time can be obtained from the proposed model more accurately. It should be noted that such phenomenological models are mathematical curve fits for the general curve type shown in Fig. 1.

Stiffness degradation can be measured directly on a test specimen. However, in realistic structures, it is easier to measure or track another variable that is tied to the stiffness. Moon et al. [26] proposed the use of natural frequencies of composite laminates as a global damage variable. The fatigue-damage state of the structure can then be measured using the so-called residual natural frequency, which could be measured from vibration tests. Badewi and Kung [27] also correlated fatigue of composite materials with changes in modal properties of select graphite epoxy composite specimens. They mention that modal properties can be used as a real-time indicator of damage in structures. Therefore, the life of the composite rotor blade can be linked with the change in system behavior of the composite rotor blade. An SHM system to predict blade life can then be developed by monitoring rotor system behavior.

In general, there are two ways to handle uncertainty in fault-detection problems. The first way is to prefilter the signals to remove the noise and outliers [28,29]. The second way is to develop robust algorithms for detecting damage in the presence of noise using estimation or soft-computing techniques. SHM systems for the composite materials are typically developed by solving an inverse problem using the changes in some measurable properties of the structure to detect damage. The inverse problem becomes complicated because of the incomplete information and uncertainty in the modeling, measurements, and signal processing. Therefore, the inverse problem for the development of an SHM system are solved using soft-computing methods such as neural network [30,31], genetic algorithm [32–34], and fuzzy logic [35–37], or by parameter estimation methods such as Kalman filtering [38]. These soft-computing methods allow the extraction of useful conclusions from slightly imprecise data. Recently, advanced soft-computing methods have been developed by hybridizing the best features of two or more soft-computing methods, and these hybridized systems are more accurate than the original ones. The genetic fuzzy system (GFS) is one of the advanced soft-computing methods developed by combining the approximate reasoning capabilities of the fuzzy systems with the learning capabilities of the genetic algorithms. The first GFS for structural-damage detection was developed by Pawar and Ganguli [39]. A genetic algorithm was used for automating the process of rule generation for a fuzzy system for application to damage detection in beam-type structures and a helicopter rotor blade. The GFS was further demonstrated for health monitoring of a thin-walled composite beam, which is conceptually similar to the composite rotor blade structure [40]. However, these studies were limited to frequencies only. In the present study, the GFS is used for developing an online SHM system using blade response, loads, and strains for composite helicopter rotor blades.

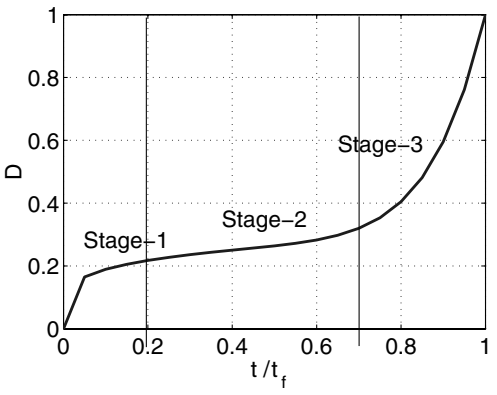

Fig. 1 Fatigue-damage growth curve.

In this paper, physics-based damage models of the composite rotor blades are developed, and the stiffness degradation of the composite blade is linked to the life consumption of the structure using curve fits based on a phenomenological fatigue-damage model. Next, an aeroelastic analysis of the damaged rotor is used to develop a fuzzy logic system, which predicts the remaining life of the structure from measured response and loads data. Two possibilities of damage occurrence in the composite rotor blade are addressed using two GFSs. The first GFS is developed for prediction of global life consumption using displacement-, force-, and moment-based measurement deltas (deviations between the undamaged and damaged blade). The second GFS is developed for prediction of local life consumption using strain-based measurement deltas. The SHM system of a composite helicopter rotor blade is demonstrated using a two-cell airfoil-section beam with stiffness properties representing a stiff in-plane helicopter rotor blade.

Analysis

The analysis of the damaged composite rotor blade is explained in three parts. The first part summarizes the mathematical model of a helicopter rotor system. The second part discusses the composite rotor blade cross-sectional analysis. The composite cross-sectional properties are included in the mathematical model of the helicopter rotor system. The third part discusses the modeling of the key damage modes in composite materials. These key damage modes are included in the mathematical model of the helicopter rotor system through the composite cross-sectional properties. A detailed formulation of the forward-flight simulation of damaged composite rotor blade is available in Pawar and Ganguli [16].

Mathematical Model of a Helicopter Rotor System

The helicopter is represented by a nonlinear model of rotating elastic rotor blades dynamically coupled to a six-degree-of-freedom rigid fuselage. Each blade undergoes flap (out-of-plane) bending, lag (in-plane) bending, elastic twist, and axial displacement. Governing equations are derived using a generalized Hamilton's principal applicable to nonconservative systems:

$$\int_{\psi_1}^{\psi_2} (\delta U - \delta T - \delta W)\, \mathrm{d}\psi = 0 \tag{1}$$

where δU and δT include energy contributions from components that are attached to the blade (pitch link, lag damper, etc.). The effects of the damaged and undamaged composite materials are included with the virtual strain energy through the elastic stiffness matrix (discussed in the next section). External aerodynamic forces on the rotor blade contribute to the virtual work variational δW. The aerodynamic forces and moments are calculated using an inflow distribution from the Bagai–Leishman free wake model and unsteady effects are accounted for using the Leishman–Beddoes model [12].

A finite element method is used to discretize the governing equation of motion and allows for the accurate representation of

complex hub kinematics and nonuniform blade properties. After finite element discretization, Hamilton's principle is written as

$$\int_{\psi_i}^{\psi_f} \sum_{i=1}^{N} (\delta U_i - \delta T_i - \delta W_i)\, \mathrm{d}\psi = 0 \tag{2}$$

Each of the beam finite elements has 15 degrees of freedom. These degrees of freedom correspond to cubic variations in axial elastic and (flap and lag) bending deflections and to quadratic variation in elastic torsion. Between the elements, there is continuity of slope and displacement for flap- and lag-bending deflections and continuity of displacements for elastic twist and axial deflections.

An aeroelastic analysis is carried out at the specified trim condition. The finite element equations representing each rotor blade are transformed to normal mode space for an efficient solution of the blade response. The nonlinear, periodic, normal mode equations are then solved for steady response using a finite element in time method. Steady and vibratory components of the rotating frame blade loads (i.e., shear forces and bending/torsion moments) are calculated using the force summation method. In this approach, blade aerodynamic and inertia forces are integrated directly over the length of the blade. Fixed-frame hub loads are calculated by summing the contributions of individual blades. A coupled trim procedure is carried out to simultaneously solve for the blade response, pilot input trim controls, and vehicle orientation. The coupled trim procedure is essential for elastically coupled blades, because elastic deflections play an important role in the steady net forces and moments generated by the rotor. For the results in this paper, all four blades are identical and have identical damage. The results are for an isolated rotor in forward flight.

Composite Rotor Blade

The composite helicopter blade is modeled as a one-dimensional, thin-walled beam undergoing extension, torsion, flap (out-of-plane), and lag (in-plane) bending, using the Chandra and Chopra [41] model. Chandra and Chopra's thin-walled composite beam model includes terms due to constrained warping torsion and terms due to transverse shear. The effects of transverse shear are included by static condensation. The restrained warping effect is negligible for a closed section and is therefore ignored for this work. The stiffness matrix of the order of (9×9) is thus reduced to a stiffness matrix of the order of (4×4) [42]:

$$\begin{bmatrix} N \\ M_x \\ -M_y \\ T_s \end{bmatrix} = \begin{bmatrix} K'_{11} & K'_{12} & K'_{13} & K'_{15} \\ & K'_{22} & K'_{23} & K'_{25} \\ \text{sym} & & K'_{33} & K'_{35} \\ & & & K'_{55} \end{bmatrix} = \begin{bmatrix} W' \\ \phi'_y \\ \phi'_x \\ \phi'_z \end{bmatrix} \tag{3}$$

The coefficients K'_{ij} of the stiffness matrix are obtained by static condensation of the (9×9) stiffness matrix $\mathbf{K}$. The terms in the $\mathbf{K}$ matrix depend on the beam cross section and geometry and are expressed in terms of the $\mathbf{A}$, $\mathbf{B}$, and $\mathbf{D}$ matrices, where $EA = K'_{11}$, $EI_y = K'_{22}$, $EI_z = K'_{33}$, and $GJ = K'_{55}$ are the axial, flap, lag, and torsion stiffness, respectively. The effects of the composite material are included in the forward-flight simulation through the strain energy expression using the cross-sectional stiffness matrix derived in this section. The effects of the key damages in composite material are included in the forward-flight simulation through the cross-sectional stiffness matrices using the progressive damage accumulation model given in the next section.

Progressive Damage Accumulation

Matrix cracking, delamination/debonding, and fiber breakage are the key damage modes in composite materials. These damage modes are modeled at the lamina and laminate level, as summarized next.

Matrix Cracking

The effects of matrix cracking in composite materials are included through the extension $\mathbf{A}$, extension-bending $\mathbf{B}$, and bending $\mathbf{D}$ stiffness matrices. The stiffness matrices for the presence of matrix cracks $\mathbf{A}^{(c)}$, $\mathbf{B}^{(c)}$, and $\mathbf{D}^{(c)}$ are obtained by subtracting the damage matrices $\Delta\mathbf{A}$, $\Delta\mathbf{B}$, and $\Delta\mathbf{D}$ from the stiffness matrices $\mathbf{A}$, $\mathbf{B}$, and $\mathbf{D}$ of the virgin laminate:

$$\mathbf{A}^{(c)} = \mathbf{A} - \Delta\mathbf{A} \tag{4}$$

$$\mathbf{B}^{(c)} = \mathbf{B} - \Delta\mathbf{B} \tag{5}$$

$$\mathbf{D}^{(c)} = \mathbf{D} - \Delta\mathbf{D} \tag{6}$$

These stiffness matrices reduce with increasing crack density. The dimensionless crack density ρ^k for the ply k is defined by

$$\rho^k = t^k / s^k \tag{7}$$

where s^k is the average crack spacing and t^k is the thickness of ply k.

The changes in stiffness matrices are obtained using the Adolfsson and Gudmundson [43] matrix-crack model, which relates the strain increment produced by an array of cracks to the total crack displacement.

Debonding/Delamination

After a certain crack density, the stiffness gets saturated at a crack density known as the saturation crack density ϕ_0. However, as damage increases, matrix cracks may induce more severe damage at the crack tip, such as debonding/delamination. The ply stiffness due to the presence of debonding/delamination can be expressed as

$$Q^M_{xx}(\phi) = rE^d_{xx}(\phi) \tag{8}$$

$$Q^M_{yy}(\phi) = rE^d_{yy}(\phi) \tag{9}$$

$$Q^M_{yx}(\phi) = r\mu^d_{xy}(\phi)E^d_{xx}(\phi) \tag{10}$$

$$Q^M_{xy}(\phi) = r\mu^d_{yx}(\phi)E^d_{xx}(\phi) \tag{11}$$

$$Q^M_{ss}(\phi) = G^d_{xy}(\phi) \tag{12}$$

where

$$r = [1 - \mu_{xy}(\phi)\mu_{yx}(\phi)]^{-1} \tag{13}$$

Stiffness reduces with increase in the effective strain ratio.

Fiber Breakage

Because fibers are the primary load-carrying elements of the fiber-reinforced composite material, fiber breakage is considered as an extreme damage. Based upon the fiber bundle theory, the effects of fiber breakage can be defined as

$$\begin{pmatrix} \bar{\sigma}_{xx} \\ \bar{\sigma}_{yy} \\ \bar{\sigma}_{xy} \end{pmatrix} = \begin{pmatrix} Q^M_{xx}(\phi) & Q^M_{xy}(\phi) & 0 \\ Q^M_{yx}(\phi) & Q^M_{yy}(\phi) & 0 \\ 0 & 0 & Q^M_{ss}(\phi) \end{pmatrix} \begin{pmatrix} d_f & 0 & 0 \\ 0 & d_f & 0 \\ 0 & 0 & d_f \end{pmatrix} \begin{pmatrix} \bar{\epsilon}_{xx} \\ \bar{\epsilon}_{yy} \\ \bar{\epsilon}_{xy} \end{pmatrix} \tag{14}$$

where d_f is the degradation coefficient for fiber breakage, which has the following form:

$$d_f = e^{-(A_f/\delta^2)^\beta} \tag{15}$$

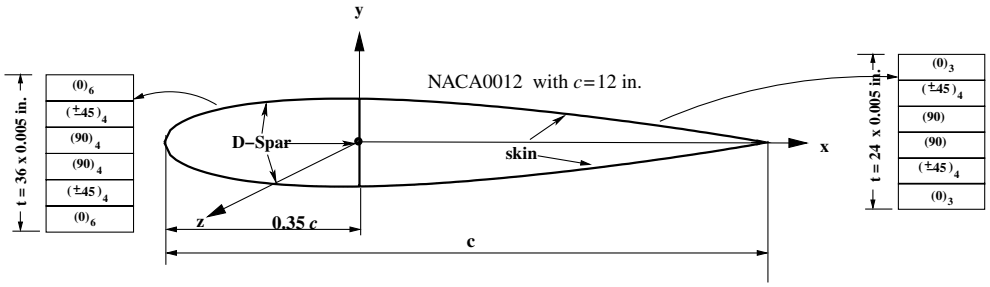

Fig. 2 Details of two-cell airfoil-section beam.

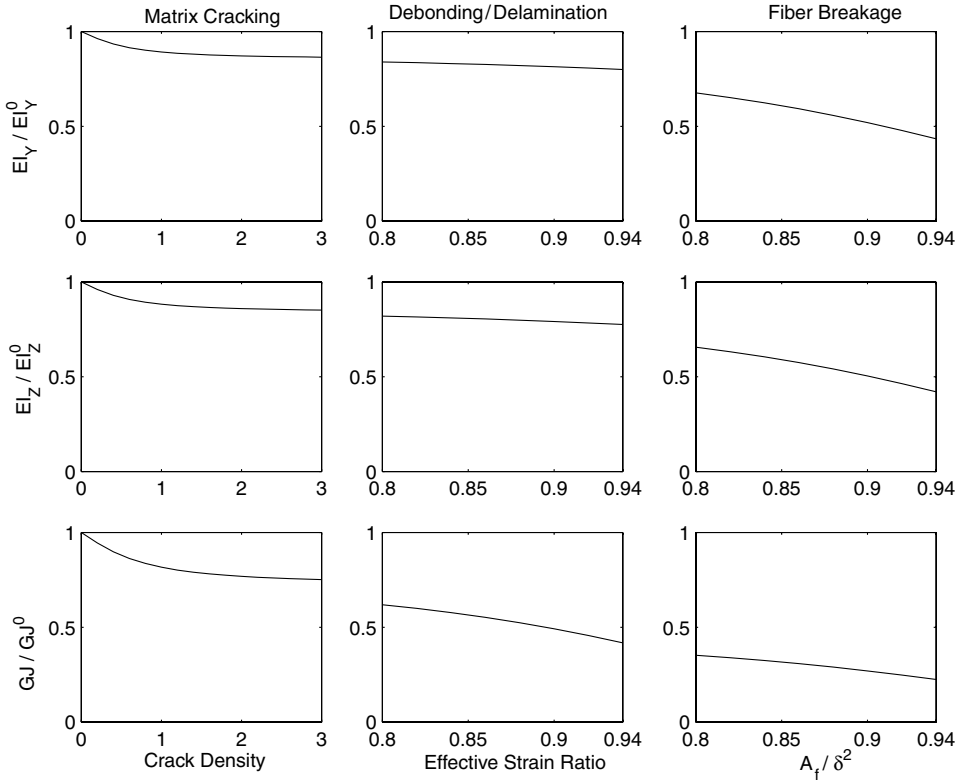

Fig. 3 Change in stiffness due to progressive damage accumulation.

Because β is a constant for a given material, d_f varies with the area ratio A_f/δ^2.

Life of the Structure

The stiffness degradation of the structure can be correlated to the life of the structure. The stiffness degradation is transformed as a function of the life of the structure based on the phenomenological theory developed for fatigue life analysis of composite materials by Mao and Mahadevan [25].

$$D = q(t/t_f)^{m_1} + (1-q)(t/t_f)^{m_2} \tag{16}$$

where $D = (E_0 - E)/(E_0 - E_f)$, E_0 is the initial stiffness $t = 0$, E_f is the stiffness at final-failure time t_f, and E is stiffness at any instant of time t. We use the functional relationship given in Eq. (16) as a curve fit to link the physics-based damage with the remaining life of the structure. Unlike other models for composite materials, the model in Eq. (16) captures the three phases of composite material degradation using one equation. Note that though Eq. (16) was originally developed to curve fit, relating the continuum damage variable D with time, it can also be used for other variables that show qualitatively similar behavior. Equation (16) is a mathematical model of curves of the type shown in Fig. 1.

The values of the curve-fitting parameters q, m_1, and m_2 are obtained by matching the stiffness-reduction values obtained by physical-damage modeling and by curve fitting Eq. (16) at the initial and final life of the structure and at the transition points of matrix cracking to debonding/delamination and debonding/delamination to fiber breakage. A detailed discussion of the transition between damage modes is given by Pawar and Ganguli [15].

Behavior of the Composite Rotor Blade

To investigate the behavior of the composite rotor blade due to life consumption, a two-cell airfoil-section beam with stiffness properties representing a stiff in-plane rotor is developed. Geometric properties and ply orientation of the two-cell airfoil section are shown in Fig. 2. Ply elastic stiffness properties are $E_L = 206$ GPa (30 msi), $E_T = 20.7$ GPa (3 msi), $G_{\mathrm{LT}} = 8.3$ GPa (1.2 msi), and $\mu_{\mathrm{LT}} = 0.3$. The length l of the blade is 5.08 m (200 in.). All of the laminates used in this paper are selected from the family of $(0/\pm 45/90)_s$ composites.

Effect on Cross-Sectional Stiffnesses

The stiffness reduction obtained due to the key damage modes are correlated to the blade life consumption. Figure 3 shows the

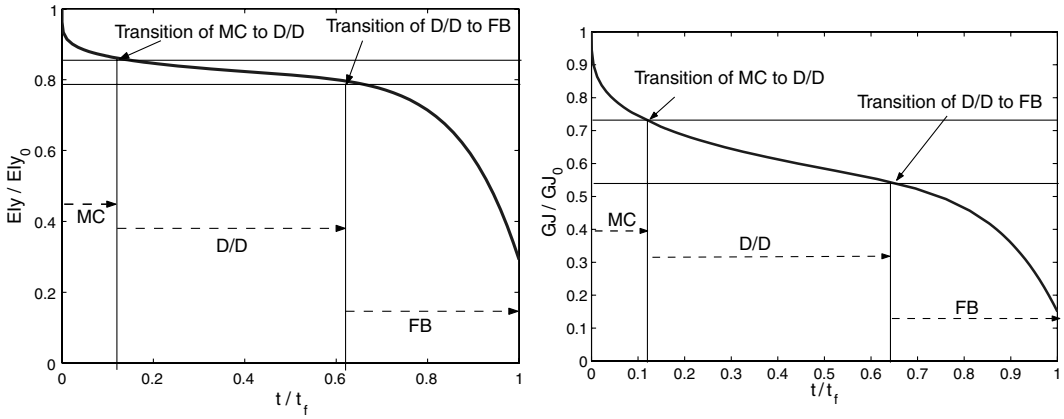

Fig. 4 Decrease in bending and torsion stiffness with increase in life consumption of the structure (MC is matrix cracking, D/D is debonding/delamination, and FB is fiber breakage).

reduction in the normalized bending and torsion cross-sectional stiffness of the two-cell airfoil-section beam due to the key damage modes. The stiffness reduction, which is a function of the physical-damage parameters, is expressed as a function of the blade life consumption using Eq. (16). Using the curve-fit equation for bending stiffness gives

$$D_1 = 0.3\left(\frac{t}{t_f}\right)^{0.2} + 0.7\left(\frac{t}{t_f}\right)^{8} \tag{17}$$

where $D_1 = (EI_{y0} - EI_y)/(EI_{y0} - EI_{yf})$, EI_{y0} is the initial bending stiffness $t = 0$, EI_{yf} is the bending stiffness at final-failure time t_f, and EI_y is the bending stiffness at any instant of time t. The same model fits the flap- and lag-bending stiffness, because degradation affects the normalized flap and lag stiffness in a similar manner.

For torsion stiffness,

$$D_2 = 0.6\left(\frac{t}{t_f}\right)^{0.3} + 0.4\left(\frac{t}{t_f}\right)^{8} \tag{18}$$

where $D_2 = (GJ_0 - GJ)/(GJ_0 - GJ_f)$, GJ_0 is the initial torsion stiffness $t = 0$, GJ_f is the torsion stiffness at final-failure time t_f, and GJ is torsion stiffness at any instant of time t. Here D_1 and D_2 can be interpreted as continuum damage variables in bending and torsion, respectively.

The bending and torsion stiffness reductions due to life consumption are shown in Fig. 4. To study the life consumption in various damage modes, the stiffness-reduction plots are divided in three zones of matrix cracking, debonding/delamination, and fiber breakage. These correspond to stages 1, 2, and 3 of the phenomenological model. From Fig. 4, it is observed that the life consumption in the matrix-cracking zone is about 12–15% of the total life. The life consumption in the debonding/delamination zone is about 45–55% of the total life, and the remaining life of the structure is covered by the final-failure fiber breakage.

Effect on Static Response

Beam stiffness provides some indication of damage growth in composites. Changes in the beam stiffness can also change parameters such as beam static response under a tip load or under gravity loads, which can be measured at periodic intervals to assess the condition of the blade. The response of the airfoil-section cantilever beam under unit static loads at the free end is obtained. Figure 5 shows an increase in the normalized tip-static responses ϕ_y (bending) and ϕ_z (torsion) of the beam, with an increase in the life consumption. Here, ϕ_y^0 and ϕ_z^0 are tip-static responses of the beams with virgin laminate. Similar to the stiffness plots, the plots of static responses are also divided into three damage zones. The life consumption of the composite blade due to matrix cracking is about 12–15% of the total life. The rate of increase in static deflection in debonding/delamination zone is very slow. At the end of the debonding/delamination zone, about 60–65% of the blade life is consumed and the fiber-breakage zone begins. Though fiber breakage is the catastrophic damage mode, the static responses show that the initial life of about 10–15% in this zone does not show a sudden

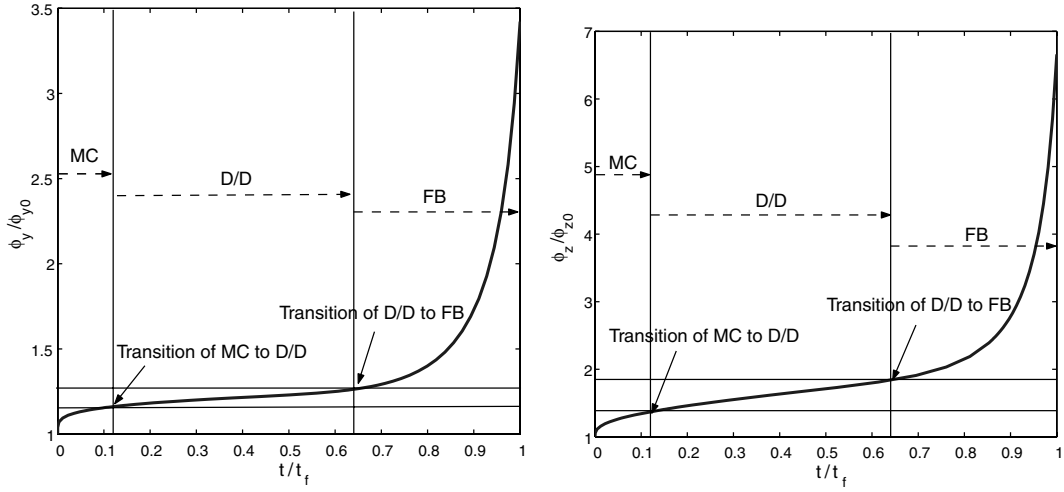

Fig. 5 Increase in tip bending and torsion response with increase in life consumption of the structure (MC is matrix cracking, D/D is debonding/delamination, and FB is fiber breakage).

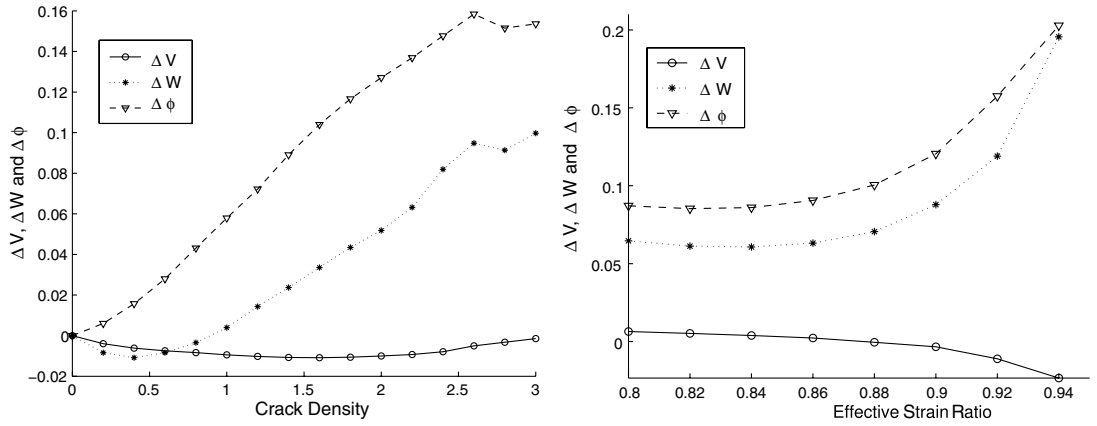

Fig. 6 Change in peak-to-peak tip lag (m), flap (m), and torsion (rad) for increasing matrix-crack density and effective strain ratio.

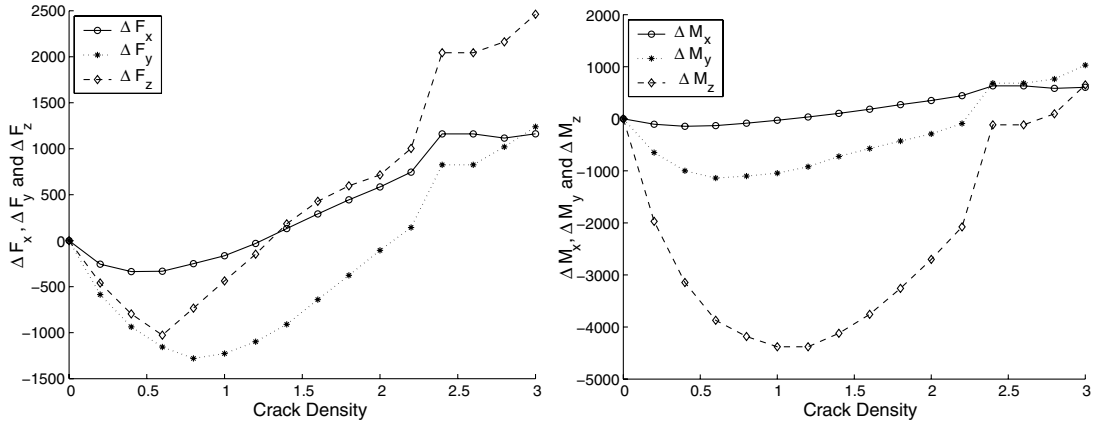

Fig. 7 Change in peak-to-peak blade root forces (N) and moments (N · m) for increasing matrix-crack density.

increase in the static response. Therefore, the structure can be conservatively kept in working condition up to the transition point of debonding/delamination to fiber breakage. A more aggressive threshold at about 70–80% of the life consumption could be used to save costs at the cost of a higher risk of failure. In general, threshold selection in health monitoring involves a tradeoff between cost and risk.

System for Predicting Life Consumption

Until now, the results focused on static variables such as stiffness and blade-tip deflection under a static loading. Obviously, there is a close relationship between stiffness and static displacements of the structure. However, static deflection cannot be used for online health monitoring. To simulate online measurements, an aeroelastic analysis of the composite rotor blade is performed. The composite damage models are integrated into the rotor aeroelastic analysis. The rotor system behavior is further linked with life consumption through the relationship between stiffness and time. The measurement deltas between a damaged and undamaged blade are used to develop two genetic fuzzy systems for the prediction of global and local physical damage and life consumption.

Numerical Simulation of Measurement Deltas

For SHM, it is important to study the effects of damage on the behavior of the structure and the changes in measurable system properties due to damage. A four-bladed, stiff in-plane hingeless composite rotor with progressive damage accumulation in the

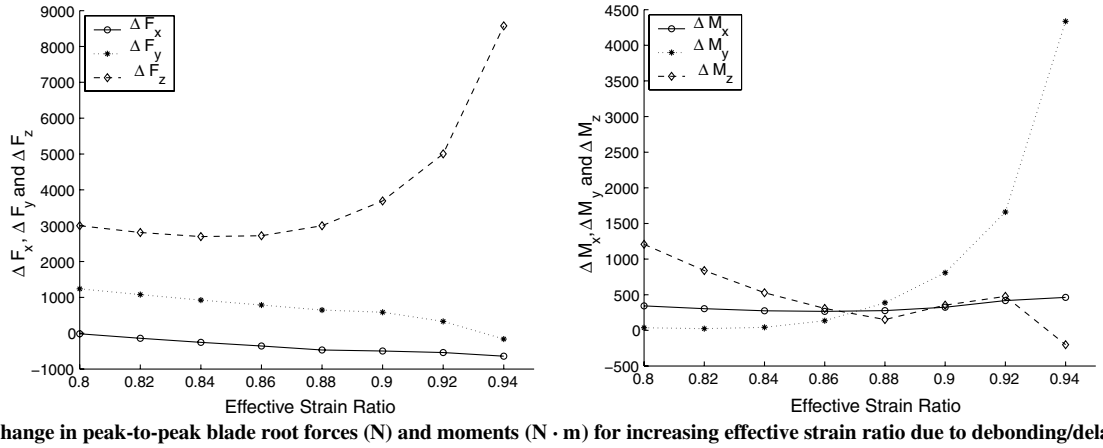

Fig. 8 Change in peak-to-peak blade root forces (N) and moments (N · m) for increasing effective strain ratio due to debonding/delamination.

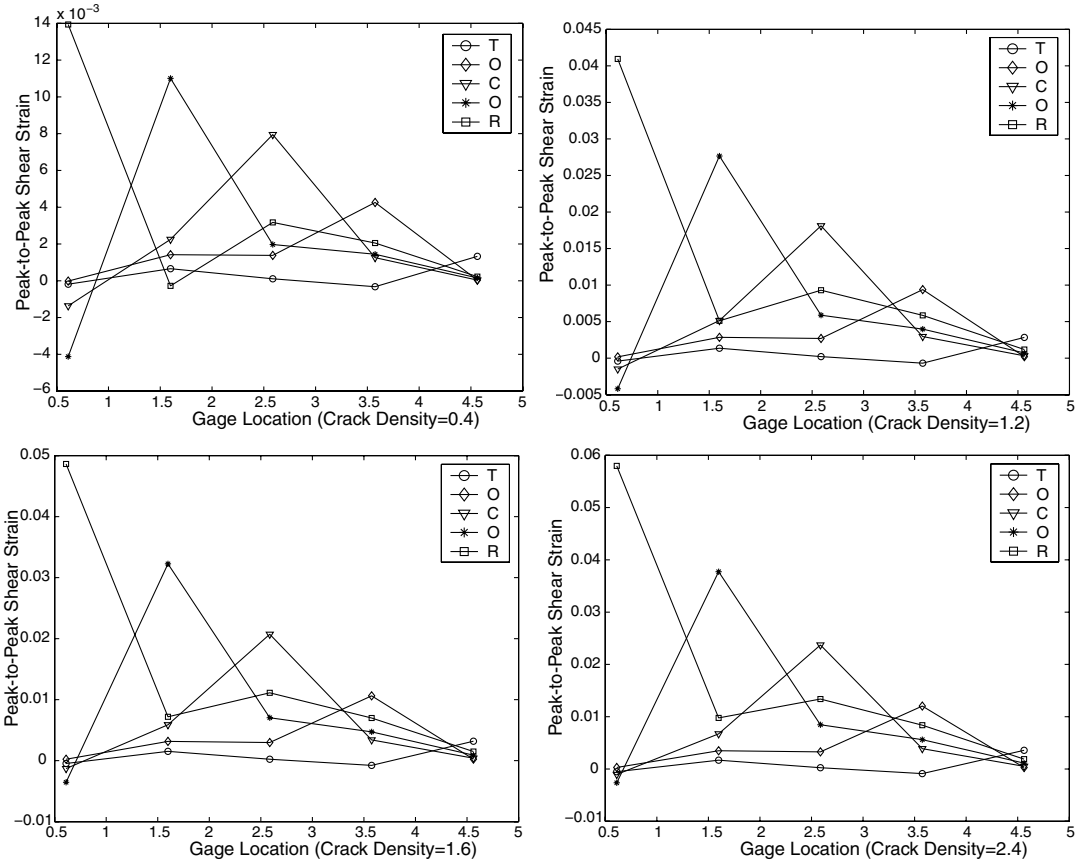

Fig. 9 Change in peak-to-peak shear strain measured at various locations for various crack densities and cracks at various locations (root is 0 m and tip is 5.08 m); crack locations are T, tip; O, outboard; C, center; I, inboard, and R, root.

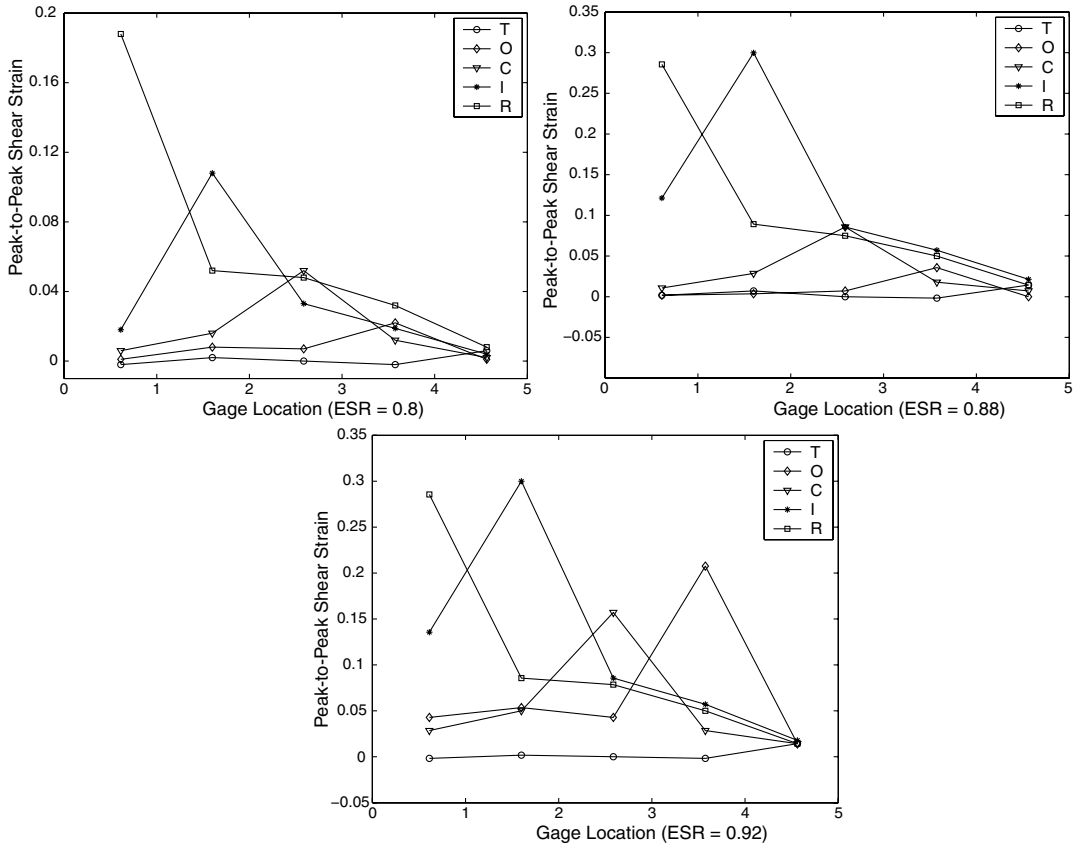

Fig. 10 Change in peak-to-peak shear strain measured at various locations for various effective strain ratios and debonding/delamination at various locations (root is 0 m and tip is 5.08 m); crack locations are T, tip; O, outboard; C, center; I, inboard, and R, root.

composite material is considered. Geometric properties and ply orientation of the two-cell airfoil section are the same as given in the previous section. Results are obtained in forward flight at an advance ratio ($\mu = V/\Omega R$) of $\mu = 0.3$, moderate thrust condition $C_T/\sigma = 0.07$, lock number $\gamma = 6.34$, and radius of gyration $mk_{m1}^2/m_0R^2 = 0.000174$, $mk_{m2}^2/m_0R^2 = 0.00061$, and $m/m_0 = 1$.

To develop the GFS, the peak-to-peak values between the undamaged and damaged rotor blade obtained at the location of maximum values of these measurements or at specific intervals are considered as measurement deltas. A detailed discussion of the effects of the key damage modes in the composite materials on various properties of the rotor blade is available in Pawar and Ganguli [16].

The measurement deltas based on deflections and forces are used to develop the global SHM system, and measurement deltas based on shear strains are used to develop the local SHM system.

Figure 6 shows the behavior of displacements in the presence of matrix cracking and debonding/delamination. There is a significant change in the flap and torsion deflections and a much smaller change in the torsion deflection. The baseline peak-to-peak lag, flap, and torsion responses of the blade are 0.1363 m, 0.1353 m, and 0.0993 rad, respectively. Figures 7 and 8 show the behavior of loads during matrix-cracking and debonding/delamination damage modes. Some of the changes are discontinuous and nonmonotonic due to the use of peak-to-peak measurements and the complicated and nonlinear helicopter dynamics and aerodynamics. It can be seen from Fig. 7 that as matrix cracking saturates near the crack density of 3, the changes in peak-to-peak deflections taper off. Also, the effect of delamination is less during the initial stages and increases near the region of transition to fiber breakage. The baseline peak-to-peak values of longitudinal, lateral, and vertical forces are 6580, 7980, and 5940 N, respectively. The baseline values of the rolling, pitching, and yawing moments are 1240, 6280, and 2115 N · m, respectively. Quite large changes in the peak-to-peak loads are therefore produced by damage. As expected, the change is much less for the matrix-cracking mode than for the delamination mode. A detailed discussion of the effects of damage on rotor system behavior is given by Pawar and Ganguli [16].

To study the effects of local damage, the peak-to-peak changes in shear strains due to matrix-cracking and debonding/delamination damage are calculated at five locations on the blade, ranging from the root to the tip. These peak-to-peak changes in shear strains are shown in Figs. 9 and 10 for matrix cracking and debonding/delamination, respectively. All of the strains are calculated on the top side of the beam and along the line passing through the point 0.35 c on a two-cell airfoil section. The maximum change in shear strain occurs where the damage occurs along the blade length in the case of local damage. Therefore, the shear strain is a useful indicator to predict damage location. For the matrix-cracking results in Fig. 9, the values of the peak-to-peak shear strains are much lower than for the rotor with debonding/delamination. Also, the values of the changes in shear strain increase with increasing crack density. For the delamination results in Fig. 10, the strains are higher than for matrix cracking and increase with the effective strain ratio. Debonding/delamination is a serious damage and leads to considerable change in the strains, compared with matrix cracking. Also, the high value of the shear strains are because they are peak-to-peak values of strains that vary considerably along the azimuth.

Fuzzy Logic System

A genetic fuzzy system is developed next, to address the issue of detecting and locating damage and the residual life of the structure in the presence of noise. The advantage of this approach over straightforward strain monitoring using thresholds is the ability to handle uncertainty in both the modeling and measurements, as well as to provide linguistic guidelines for maintenance that are more useful for practical applications and less prone to thresholding errors. Before developing the genetic fuzzy system, a brief description of a fuzzy logic system is given in this section. Fuzzy logic is a unique soft-computing method that simultaneously handles numerical data and linguistic knowledge. A fuzzy logic system is a nonlinear mapping of an input feature vector into a scalar output [44]. Fuzzy set theory and fuzzy logic provide the framework for the nonlinear mapping. Fuzzy logic systems have been widely used in engineering applications because of the flexibility they offer designers and their ability to handle uncertainty. A fuzzy logic system can be expressed as a linear combination of fuzzy basis functions and is a universal function approximator. The schematic diagram of fuzzy logic is shown in Fig. 11 for $\Delta\omega$ as crisp inputs and *damage* and *damage location* as crisp outputs. Here, $\Delta\omega$ is a measurement delta that can be changed in frequency between the undamaged and damaged

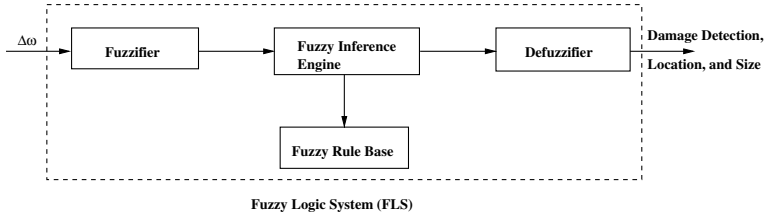

Fig. 11 Schematic representation of a fuzzy logic system.

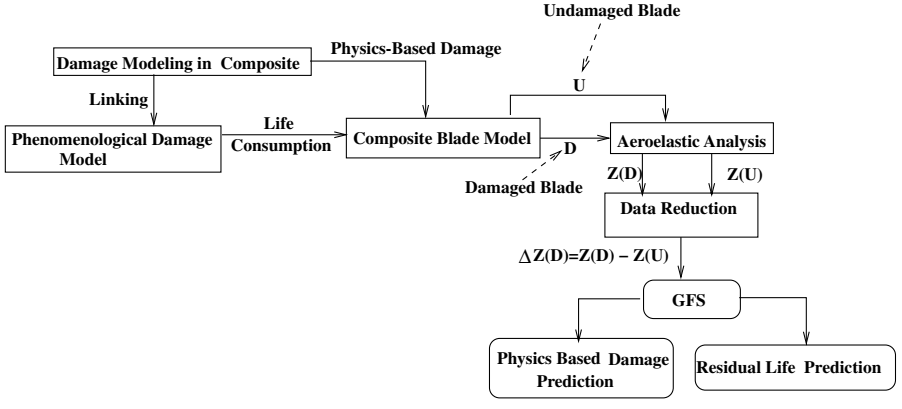

Fig. 12 Schematic representation of development of SHM.

Table 1 Linguistic classification of damage for the genetic fuzzy system for global damage detection

No.	Physics-based rule	Damage level	Life con (res life)	Prog action
1	Undamaged	Nil crack density	Nil (100%)	OK
2	Very small crack density	Crack density 0–0.8	0–2.5% (97.5%)	OK
3	Small crack density	Crack density 0.8–1.2	2.5–5% (95%)	OK
4	Considerable crack density	Crack density 1.2–1.6	5–7% (93%)	OK
5	High crack density	Crack density 1.6–2.0	7–8.5%(91.5%)	OK
6	Very high crack density	Crack density 2.0–2.4	8.5–10% (90%)	OK
7	Saturation crack density	Crack density 2.4–3.0	10–12 % (88%)	OK
8	Transition of MC to D/D[a]	CD 3.0[b] to ESR 0.8[c]	12–20% (80%)	Watch
9	Slight D/D	ESR 0.8–0.88	20–43% (67%)	Watch
10	Moderate D/D	ESR 0.88–0.9	43–50%(50%)	Watch
11	Severe D/D	ESR 0.9–0.92	50–56% (44%)	Watch
12	Extreme D/D	ESR 0.92–0.94	56–62% (38%)	Remove

[a]MC denotes matrix cracking and D/D denotes debonding/delamination.
[b]Saturation crack density.
[c]The effective strain ratio (ESR) at which the effects of D/D become considerable prognostic actions: 1) blade is OK, no action is required; 2) put the blade under watch, and 3) remove the blade; take for thorough inspection.

structure, for example. It could also be changed in strains, blade-tip responses, and loads in a helicopter rotor blade.

A typical fuzzy logic system maps crisp inputs to crisp outputs using four basic components: rules, fuzzifier, inference engine, and defuzzifier. Rules can come from experts or can be obtained from numerical data. In either case, engineering rules are expressed as a collection of IF–THEN statements such as "IF u_1 is HIGH and u_2 is LOW, THEN v is LOW."

The fuzzifier maps crisp input numbers into fuzzy sets. It is needed to activate rules that are expressed in terms of linguistic variables. An inference engine of the fuzzy logic system maps fuzzy sets to fuzzy sets and determines the way in which the fuzzy sets are combined. In several applications, crisp numbers are needed as an output of the fuzzy logic system. In those cases, a defuzzifier is used to calculate crisp values from fuzzy values.

Two aspects in the design of the fuzzy system are difficult: 1) generating the best rule set and 2) tuning the membership functions. The rules and the membership functions must accurately capture the relationship between the independent and dependent variable.

Unfortunately, the tasks of tuning membership function and generating rules are not independent. The task of selecting membership functions and rule values is difficult, because the information has to be obtained from numerical data of the system to be modeled.

Another problem is selecting an appropriate number of fuzzy sets. Most studies use experience to come up with this number. The problems in the design of a fuzzy system can be addressed by using a learning algorithm such as the genetic algorithm. This leads to the genetic fuzzy system for which the design for the rotor SHM problem is discussed in the nest section.

Development of a Genetic Fuzzy System

There are two possibilities of damage in composite rotor blades. The first possibility is that the damage will be approximately uniform along the whole blade, which may occur due to the vibrating environment of the helicopter. The second possibility is that the damage will be localized, which may occur due to a sudden impact by a foreign object or due to an uneven loading condition. In this section, two GFSs are formulated. The first or global GFS is for predicting the physical damage and life consumption in the matrix-cracking and debonding/delamination zones along the whole blade. The second or local GFS is for predicting the physical damage and life consumption in the matrix-cracking and debonding/delamination zones in various parts of the blade. The fiber-breakage damage mode in composite materials is considered as a catastrophic damage mode, and detection of such a damage is not useful. Therefore, fiber breakage is not considered when designing the GFS.

The schematic diagram of the SHM system development process is shown in Fig. 12. The difference between the global and local SHM systems lies in the choice of sensor measurement **z** in Fig. 12, as discussed next.

Global Damage Detection

The global damage detection system is developed to predict the physical damage and life consumption along the whole blade.

Input and Ouput. Inputs to the global GFS are measurement deltas based on displacement, force, and moment. The outputs of the global GFS are various damage levels in the matrix-cracking and debonding/delamination zones. The objective is to find the mapping between the measurement deltas and various damage levels.

Fuzzification. In this fuzzy system, physical-damage parameters and life-consumption parameters in the matrix-cracking and debonding/delamination zones are crisp numbers. To get a degree of resolution of the extent of physical damage and life consumption, the physical-damage parameter and life-consumption parameter are allowed to have several zones based on the physical damage and split into linguistic variables, as shown in Table 1. These classifications are based on the numerical results obtained for matrix cracking and

Table 2 Linguistic classification of damage for local damage detection

Damage name	Damage level	Life con (res life)	Prog action[b]
Undamaged	Matrix-crack density zero	Nil (100%)	OK
Small crack density	Matrix-crack density 0.4	About 2% (98%)	OK
Moderate crack density	Matrix-crack density 1.2	About 5% (95%)	OK
High crack density	Matrix-crack density 1.6	About 7% (93%)	OK
Very high crack density	Matrix-crack density 2.4	About 10% (90%)	OK
Slight D/D[a]	ESR 0.8	About 20% (80%)	Watch
Moderate D/D	ESR 0.88	About 43% (67%)	Watch
Severe D/D	ESR 0.92	About 56% (44%)	Remove

[a]D/D denotes debonding/delamination.
[b]Prognostic actions: 1) blade is OK, no action is required; 2) put the blade under watch, and 3) remove the blade; take for thorough inspection.

Table 3 Midpoints and standard deviations of rules for the genetic fuzzy system for global damage detection

No.	ΔW	$\Delta\phi$	ΔF_x	ΔF_y	ΔF_z	ΔM_x	ΔM_y	ΔM_z
1	0.00 (0.10)	0.00 (0.12)	0.00 (0.19)	0.00 (0.16)	0.00 (0.14)	0.00 (0.18)	0.00 (0.12)	0.00 (0.19)
2	−0.07 (0.11)	0.09 (0.13)	−0.11 (0.13)	−0.52 (0.17)	−0.05 (0.14)	−0.07 (0.16)	−0.18 (0.19)	−0.49 (0.13)
3	0.03 (0.17)	0.32 (0.11)	−0.12 (0.15)	−0.96 (0.18)	−0.06 (0.17)	−0.04 (0.17)	−0.34 (0.19)	−1.00 (0.17)
4	0.15 (0.11)	0.49 (0.11)	0.11 (0.12)	−0.70 (0.16)	0.02 (0.13)	0.18 (0.11)	−0.25 (0.15)	−0.95 (0.13)
5	0.27 (0.17)	0.64 (0.17)	0.38 (0.16)	−0.30 (0.15)	0.08 (0.13)	0.43 (0.13)	−0.14 (0.20)	−0.75 (0.12)
6	0.42 (0.10)	0.76 (0.15)	0.75 (0.13)	0.29 (0.15)	0.20 (0.18)	0.80 (0.19)	0.07 (0.15)	−0.33 (0.15)
7	0.57 (0.14)	0.84 (0.17)	1.00 (0.19)	0.83 (0.19)	0.33 (0.14)	1.00 (0.18)	0.29 (0.12)	0.06 (0.14)
8	0.51 (0.16)	0.67 (0.17)	0.49 (0.13)	1.00 (0.16)	0.40 (0.13)	0.77 (0.19)	0.18 (0.13)	0.22 (0.15)
9	0.42 (0.17)	0.52 (0.15)	−0.21 (0.14)	0.76 (0.11)	0.44 (0.16)	0.50 (0.13)	0.07 (0.11)	0.16 (0.18)
10	0.50 (0.15)	0.61 (0.18)	−0.42 (0.16)	0.50 (0.18)	0.49 (0.16)	0.49 (0.13)	0.20 (0.18)	0.06 (0.19)
11	0.65 (0.14)	0.77 (0.11)	−0.45 (0.16)	0.37 (0.18)	0.64 (0.16)	0.60 (0.16)	0.41 (0.20)	0.10 (0.18)
12	0.98 (0.19)	1.00 (0.12)	−0.51 (0.10)	0.07 (0.18)	1.00 (0.11)	0.71 (0.20)	1.00 (0.12)	0.03 (0.17)

Table 4 Success rate for various testing noise level and training noise level of 0.15 for global damage detection using displacement and force

	Displacements				Forces			
No.	$S_{R0.05}$	$S_{R0.1}$	$S_{R0.15}$	$S_{R0.20}$	$S_{R0.05}$	$S_{R0.1}$	$S_{R0.15}$	$S_{R0.20}$
1	96.90	79.70	69.90	60.20	100.00	100.00	99.60	95.50
2	97.80	81.60	68.70	50.50	100.00	100.00	97.00	90.30
3	100.00	97.50	77.60	65.10	100.00	100.00	99.70	95.90
4	100.00	81.20	46.10	29.10	100.00	100.00	89.30	66.30
5	100.00	92.40	69.40	49.90	100.00	100.00	100.00	100.00
6	98.10	61.40	35.50	24.40	100.00	100.00	100.00	99.80
7	97.70	73.60	55.10	41.70	100.00	100.00	100.00	100.00
8	80.90	48.80	27.80	21.10	100.00	100.00	100.00	100.00
9	98.40	73.90	60.40	48.20	100.00	100.00	96.40	91.30
10	82.30	46.60	31.60	23.70	100.00	97.20	88.30	78.00
11	94.50	66.00	46.90	34.00	100.00	91.30	76.30	63.90
12	100.00	100.00	100.00	96.60	100.00	100.00	100.00	96.60
Avg	95.55	75.23	57.42	45.38	100.00	99.04	95.55	89.80
Min	80.90	46.60	27.80	21.10	100.00	91.30	76.30	63.90

debonding/delamination. The displacement measurement deltas are first considered for defining the rules, because they show approximately monotonic behavior with respect to matrix cracking and debonding/delamination (Fig. 6). Next, the force and moment measurement deltas (Figs. 7 and 8) are considered for prediction of matrix cracking and debonding/delamination. The first step in fuzzy logic is to transform typical measurements into fuzzy linguistic measures. This is done using the relation between peak-to-peak displacements and physical-damage parameters, shown in Fig. 6. Table 1 shows the linguistic and numerical measures based on the displacement measurement deltas. This table also shows the relation between the physical-damage parameters and the life-consumption parameters of the composite rotor blade. The linguistic classifications allow the damage parameters and life-consumption parameters to be grouped into small levels that are more robust to the presence of uncertainty and also provide a fuzzy rule base that is similar to human reasoning. The different levels of damage can be used to create different alarm levels to be shown to the user.

The measurement deltas ΔW, $\Delta\phi$, ΔF_x, ΔF_y, ΔF_z, ΔM_x, ΔM_y, and ΔM_z are treated as fuzzy variables. Fuzzy sets with Gaussian membership functions are used to define these input variables. The Gaussian membership function can be written as

Table 5 Success rate for various testing noise level and training noise level of 0.15 for global damage detection using moments and all measurements

	Moments				All			
No.	$S_{R0.05}$	$S_{R0.1}$	$S_{R0.15}$	$S_{R0.20}$	$S_{R0.05}$	$S_{R0.1}$	$S_{R0.15}$	$S_{R0.20}$
1	100.00	100.00	100.00	97.50	100.00	100.00	100.00	100.00
2	100.00	100.00	100.00	96.40	100.00	100.00	100.00	99.90
3	100.00	99.90	94.70	90.60	100.00	100.00	100.00	99.30
4	100.00	94.90	74.30	45.80	100.00	100.00	98.30	90.20
5	100.00	100.00	99.90	97.80	100.00	100.00	100.00	100.00
6	100.00	100.00	99.50	89.60	100.00	100.00	100.00	100.00
7	100.00	100.00	95.50	89.00	100.00	100.00	100.00	100.00
8	100.00	99.80	87.00	68.00	100.00	100.00	100.00	99.50
9	100.00	91.40	75.40	60.80	100.00	100.00	95.30	86.30
10	100.00	93.20	76.70	65.20	100.00	100.00	98.90	94.40
11	100.00	97.40	79.70	67.70	100.00	100.00	98.00	94.60
12	100.00	100.00	100.00	100.00	100.00	100.00	100.00	100.00
Avg	100.00	98.05	90.23	80.70	100.00	100.00	99.21	97.02
Min	100.00	91.40	74.30	45.80	100.00	100.00	95.30	86.30

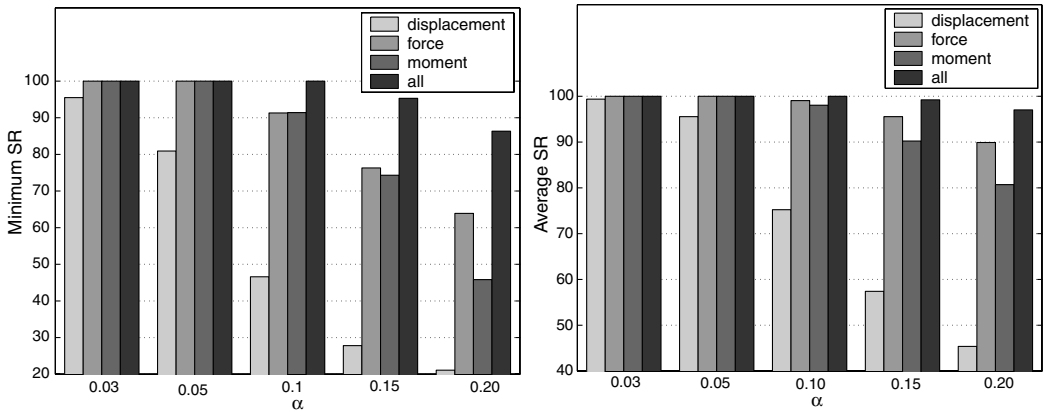

Fig. 13 Effect of various measurements on the minimum and average success rates of a genetic fuzzy logic system for global damage detection.

$$\mu(x) = e^{-0.5(\frac{x-m}{\sigma})^2} \tag{19}$$

were m is the midpoint and σ is the standard deviation. Gaussian fuzzy sets have the advantage of providing smooth transition between the different sets [44]. Furthermore, they always have nonzero values on the real number line, and therefore every rule in the fuzzy system fires to some degree. Changes in the measurement deltas are calculated using the aeroelastic analysis for different levels of damages along the whole blade. The midpoints of the Gaussian function are calculated by normalizing the changes in measurement deltas with their maximum values. The GFS is tested using the normalized noisy measurement delta x, which is derived from the noise model given as

$$x = m + u\alpha \tag{20}$$

The addition of noise to the simulations is needed to make it realistic and to develop a robust model-based diagnostic system. A noise-level parameter α defines the maximum variance between the computed value of m (normalized) and simulated measured value x (normalized), which is a simulation of the practical measurement.

Rule Generation. Rules for the fuzzy system are obtained by fuzzification of the numerical values obtained from an aeroelastic analysis of the composite helicopter blade in forward flight. The fuzzy sets corresponding to ΔW, $\Delta\phi$, ΔF_x, ΔF_y, ΔF_z, ΔM_x, ΔM_y,

Table 6 Midpoints and standard deviations of rules for local damage detection using strain-based measurement deltas

No.	Rule	$\Delta\epsilon_{\text{Tip}}$	$\Delta\epsilon_{\text{Outboard}}$	$\Delta\epsilon_{\text{Center}}$	$\Delta\epsilon_{\text{Inboard}}$	$\Delta\epsilon_{\text{Root}}$
1	Undamaged	0 (0.18)	0 (0.14)	0 (0.17)	0 (0.13)	0 (0.15)
2	Small CD at the tip	0.08 (0.13)	−0.00 (0.16)	0.00 (0.10)	0.00 (0.13)	−0.00 (0.13)
3	Small CD at the outboard	0.00 (0.19)	0.02 (0.11)	0.01 (0.14)	0.00 (0.16)	−0.00 (0.16)
4	Small CD at the center	0.00 (0.16)	0.01 (0.10)	0.05 (0.15)	0.01 (0.16)	−0.00 (0.16)
5	Small CD at the inboard	0.01 (0.13)	0.01 (0.14)	0.01 (0.19)	0.04 (0.13)	−0.01 (0.12)
6	Small CD at the root	0.01 (0.14)	0.01 (0.12)	0.02 (0.13)	−0.00 (0.13)	0.05 (0.18)
7	Moderate CD at the tip	0.17 (0.12)	−0.00 (0.17)	0.00 (0.18)	0.00 (0.16)	−0.00 (0.15)
8	Moderate CD at the outboard	0.01 (0.11)	0.05 (0.13)	0.02 (0.20)	0.01 (0.19)	0.00 (0.19)
9	Moderate CD at the center	0.02 (0.10)	0.01 (0.18)	0.11 (0.12)	0.02 (0.12)	−0.00 (0.19)
10	Moderate CD at the inboard	0.04 (0.13)	0.02 (0.18)	0.04 (0.14)	0.09 (0.12)	−0.01 (0.18)
11	Moderate CD at the root	0.07 (0.19)	0.03 (0.13)	0.06 (0.18)	0.02 (0.14)	0.13 (0.16)
12	High CD at the tip	0.19 (0.20)	−0.00 (0.11)	0.00 (0.14)	0.01 (0.17)	−0.00 (0.17)
13	High CD at the outboard	0.01 (0.17)	0.05 (0.19)	0.02 (0.15)	0.01 (0.17)	0.00 (0.15)
14	High CD at the center	0.02 (0.11)	0.02 (0.11)	0.13 (0.15)	0.02 (0.19)	−0.00 (0.20)
15	High CD at the inboard	0.05 (0.17)	0.02 (0.12)	0.04 (0.20)	0.11 (0.17)	−0.01 (0.18)
16	High CD at the root	0.09 (0.13)	0.03 (0.18)	0.07 (0.12)	0.02 (0.11)	0.16 (0.11)
17	Very high CD at the tip	0.21 (0.17)	−0.00 (0.18)	0.00 (0.17)	0.01 (0.19)	−0.00 (0.12)
18	Very high CD at the outboard	0.02 (0.14)	0.06 (0.14)	0.02 (0.14)	0.01 (0.17)	0.00 (0.12)
19	Very high CD at the center	0.03 (0.14)	0.02 (0.19)	0.15 (0.17)	0.02 (0.18)	−0.00 (0.13)
20	Very high CD at the inboard	0.07 (0.15)	0.03 (0.19)	0.05 (0.17)	0.13 (0.14)	−0.01 (0.14)
21	Very high CD at the root	0.11 (0.17)	0.04 (0.14)	0.08 (0.14)	0.03 (0.19)	0.19 (0.17)
22	Slight D/D at the tip	0.41 (0.16)	−0.01 (0.15)	0.00 (0.16)	0.01 (0.14)	−0.00 (0.11)
23	Slight D/D at the outboard	0.04 (0.16)	0.12 (0.15)	0.03 (0.10)	0.02 (0.15)	0.00 (0.10)
24	Slight D/D at the center	0.10 (0.12)	0.04 (0.13)	0.33 (0.16)	0.05 (0.14)	0.01 (0.11)
25	Slight D/D at the inboard	0.28 (0.17)	0.09 (0.16)	0.18 (0.19)	0.36 (0.18)	0.06 (0.16)
26	Slight D/D at the root	0.48 (0.14)	0.15 (0.19)	0.31 (0.12)	0.18 (0.15)	0.62 (0.16)
27	Moderate D/D at the tip	0.59 (0.19)	−0.01 (0.20)	0.00 (0.12)	0.01 (0.17)	−0.00 (0.18)
28	Moderate D/D at the outboard	0.07 (0.20)	0.18 (0.11)	0.05 (0.17)	0.03 (0.10)	0.01 (0.18)
29	Moderate D/D at the center	0.23 (0.15)	0.08 (0.12)	0.59 (0.15)	0.09 (0.10)	0.04 (0.13)
30	Moderate D/D at the inboard	0.42 (0.20)	0.13 (0.20)	0.27 (0.19)	0.51 (0.12)	0.12 (0.19)
31	Moderate D/D at the root	0.83 (0.15)	0.24 (0.18)	0.48 (0.15)	0.31 (0.18)	0.94 (0.12)
32	Severe D/D at the tip	0.76 (0.13)	−0.01 (0.11)	0.00 (0.11)	0.02 (0.16)	−0.01 (0.11)
33	Severe D/D at the outboard	0.64 (0.17)	1.00 (0.19)	0.27 (0.13)	0.19 (0.15)	0.15 (0.12)
34	Severe D/D at the center	0.48 (0.11)	0.15 (0.17)	1.00 (0.15)	0.18 (0.15)	0.12 (0.12)
35	Severe D/D at the inboard	1.00 (0.18)	0.28 (0.15)	0.54 (0.14)	1.00 (0.20)	0.40 (0.10)
36	Severe D/D at the root	0.88 (0.14)	0.26 (0.19)	0.51 (0.13)	0.33 (0.14)	1.00 (0.17)

Table 7 Success rate of various rules for local damage detection using strain-based measurement deltas

Rule no.	$S_{R0.03}$	$S_{R0.05}$	$S_{R0.10}$
1	100.00	100.00	100.00
2	100.00	100.00	100.00
3	100.00	100.00	100.00
4	100.00	100.00	100.00
5	100.00	100.00	100.00
6	100.00	100.00	100.00
7	100.00	98.60	81.10
8	100.00	99.60	81.50
9	100.00	99.90	86.00
10	100.00	100.00	95.50
11	100.00	100.00	99.90
12	100.00	99.90	47.20
13	100.00	100.00	84.20
14	100.00	99.80	68.40
15	100.00	100.00	96.10
16	100.00	100.00	83.80
17	100.00	99.30	84.10
18	100.00	97.70	69.20
19	100.00	100.00	89.90
20	100.00	100.00	93.50
21	100.00	100.00	99.40
22	100.00	100.00	100.00
23	100.00	100.00	100.00
24	100.00	100.00	100.00
25	100.00	100.00	100.00
26	100.00	100.00	100.00
27	100.00	100.00	100.00
28	100.00	100.00	100.00
29	100.00	100.00	100.00
30	100.00	100.00	100.00
31	99.90	92.90	74.90
32	100.00	100.00	86.00
33	100.00	100.00	100.00
34	100.00	100.00	100.00
35	100.00	100.00	100.00
36	99.90	91.80	73.90
Avg	99.99	99.43	91.52
Min	99.90	91.80	47.20

and ΔM_z are generated by taking the change in measurements obtained from the aeroelastic analysis solution as midpoints of membership functions corresponding to a damage level.

For each measurement delta corresponding to a given damage level, the degree of membership in the fuzzy set is calculated. Each measurement delta is assigned to the fuzzy set with the maximum degree of membership. One rule is obtained for each damage level by relating the measurement deltas. The standard deviation is obtained by maximizing the success rate for each set.

The fuzzy rules provide a knowledge base and represent how a human engineer would interpret data to isolate a damage level using measurement deltas. The fuzzy rules represent a fuzzified model of the measurements obtained by an aeroelastic analysis for each damage level. Because Gaussian fuzzy sets asymptotically approaching zero far from the midpoint are used, all of the rules fire at some level. For any given input set of measurement deltas, the fuzzy rules are applied using product implication. Once the fuzzy rules are applied for a given measurement, we have degrees of membership for each of the damage levels. For damage-level isolation, we are interested in the most likely damage level. The damage level with the highest degree of membership is selected as the most likely damage level.

Tuning of the Rules. The realistic measurement deltas will be noisy due to vibrating environment of the helicopter. By generating noisy measurement deltas and testing the fuzzy system for a known damage, we can define a success rate. For example, if N is the total number of classifications and N_c is the number of correct classifications, the success rate can be defined as

$$S_R = (N_c/N)100 \tag{21}$$

The success rate of the GFS is calculated by using N number of noisy training samples. Because the midpoints of the fuzzy sets are tuned using the aeroelastic analysis, the success rate is a function of the standard deviations of the Gaussian functions for the fuzzy system, that is,

$$S_R = S_R(\sigma_{ij}) \tag{22}$$

To get a better performance in this environment, the fuzzy system is tuned with noisy measurement deltas. The uncertainty associated with variables (i.e., standard deviation of the Gaussian membership functions) is calculated using a genetic algorithm for optimization of the success rate:

$$\begin{aligned} &\text{maximize } S_R(\sigma_{ij}) \quad \text{for } \sigma^{\min} \le \sigma_{ij} \le \sigma^{\max}, \\ &i = 1, 2, \cdots, M \quad \text{and} \quad j = 1, 2, \cdots, P \end{aligned} \tag{23}$$

where M is the number of rules and P is the number of measurements. Therefore, the success rate of the GFS is the objective function, and the standard deviations σ corresponding to each rule are the design variables for the genetic algorithm. The use of formal optimization to design the fuzzy system leads to an optimal diagnostic system that provides the best results for the given structure, measurement set, and noise level in the data.

Local Damage Detection

The local damage detection system is developed to predict the damage at various locations along the blade.

Input and Output. Inputs to the local GFS are strain-based measurement deltas at five locations, and outputs are physical-damage parameters and life-consumption parameters at different locations. The objective is to find a mapping between the measurement deltas and physical-damage parameters and life-consumption parameters at five different locations.

Fuzzification. In this fuzzy system, physical-damage parameters and life-consumption parameters at a given location are crisp numbers. The different locations considered are as follows: the tip ranges from 0 to 20% of the blade from the free end, the outboard from 20 to 40%, the center from 40 to 60%, the inboard from 60 to 80%, and the root from 80 to 100%.

To get a degree of resolution of the extent of physical damage and life consumption, physical-damage parameters and life-consumption parameters at each location are allowed several levels and split into linguistic variables. Fuzzy logic rules are defined based on the

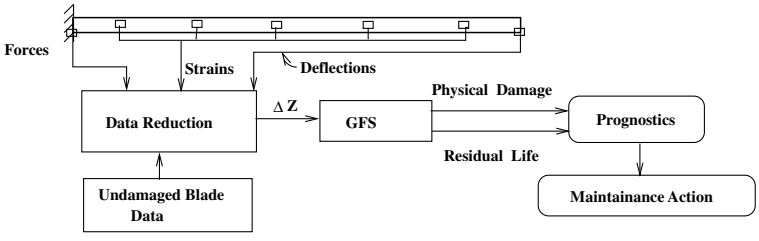

Fig. 14 Schematic representation of implementation of SHM.

shear strains obtained for a few key physical-damage parameters. These shear strains are first obtained for physical-damage parameters and then linked with the life of the blade. The linguistic relations of the key life-consumption parameters and physical-damage parameters are shown in Table 2.

Strain-based measurement deltas $\triangle\epsilon_{\text{Tip}}$, $\triangle\epsilon_{\text{Outboard}}$, $\triangle\epsilon_{\text{Center}}$, $\triangle\epsilon_{\text{Inboard}}$, and $\triangle\epsilon_{\text{Root}}$ are treated as fuzzy variables. Fuzzy sets with Gaussian membership functions are used to define these input variables. Change in strains (measurement deltas) is calculated using an aeroelastic analysis for a combination of five different locations and seven different levels of damages and are shown in Figs. 9 and 10. Formulation of the GFS system and calculation of the success rate is done using the algorithm discussed in the previous section.

Testing of GFS

The global and local GFS are tested at various noise levels. All of the measurements are normalized with their maximum value.

Global Damage Detection

The midpoints and standard deviations of the Gaussian membership functions for the rules underlying the global GFS with a training noise level of 0.15 are given in Table 3. Success rates of the GFS are calculated for various noise levels of 0.03, 0.05, 0.10, 0.15, and 0.20. The GFS is tested using four sets of measurement deltas, namely: displacement-, force-, and moment-based measurements deltas and all measurement deltas together. Tables 4 and 5 show the success rates for all of the rules for four different sets of measurement deltas at various noise levels and these results are summarized in Fig. 13.

From Tables 4 and 5 and Fig. 13, it is observed that the GFS with displacement-based measurement deltas gives good results at the noise level of 0.05, with an average success rate of 95.55% and a minimum success rate of 80.90% transition of matrix cracking to D/D) and starts deteriorating rapidly with a further increase in noise level.

The GFS with force-based measurement deltas gives a success rate of 100% at the noise level of 0.05. For a noise level of 0.1, the GFS with force-based measurement deltas gives an average success rate of 99% and a minimum success rate of 91.3% (severe debonding/delamination) and starts falling for higher noise levels of 0.15 and 0.20 by giving average success rates of 96 and 89.8% and minimum success rates of 76 and 63.90%, respectively.

The GFS with moment-based measurement deltas gives a success rate of 100% at the noise level of 0.05. For a noise level of 0.1, the GFS with moment-based measurement deltas gives an average success rate of 98.05% and a minimum success rate of 91.4% (slight debonding/delamination) and starts falling for higher noise levels of 0.15 and 0.20 by giving average success rates of 96 and 89.8%, respectively, and minimum success rates of 76 and 63.90%, respectively.

When all measurement deltas are considered for matrix-cracking and debonding/delamination detection, the GFS gives a success rate of 100% up to a noise level of 0.10 and also gives good results with higher noise levels of 0.15 and 0.20 by giving average success rates of 99.21 and 97.02%, respectively, and minimum success rates of 95.30 and 86.30%, respectively. Thus, the use of both displacement- and load-based measurements results in a health-monitoring system with high levels of accuracy, even with noisy data.

Localized Damage Detection

The midpoints and standard deviations of the Gaussian membership functions for the local GFS rules are tabulated in Table 6. These results are obtained at a training noise level of 0.05, which is found to be good for the strain-based measurement deltas. The midpoints in this table are normalized with the maximum value of the corresponding measurement deltas, and corresponding values of the standard deviations are given in parentheses.

The success rates for prediction of physical damage and life consumption at various parts of the blades are tested at noise levels of 0.03, 0.05, and 0.10. Table 7 shows the success rate for all of the rules with various noise levels. From Table 7, it is observed that the local GFS gives a success rate of 100% up to a noise level of 0.03. For debonding/delamination zone, the GFS gives a success rate of 100% for a noise level of 0.03, except for two rules: moderate debonding/delamination at the root and severe debonding/delamination at the root. For a noise level of 0.05, the GFS gives an average success rate of 99.42% and a minimum success rate of 91.8%. The GFS gives a minimum success rate of 97.70% for the matrix-crack zone and a minimum success rate of 91.8% for the debonding/delamination zone for a noise level of 0.05. It can be noted that the GFS gives a success rate of 100% for debonding/delamination zone up to a noise level of 0.05, except for two rules: moderate debonding/delamination at the root and severe debonding/delamination at the root. However, for a higher noise level of 0.1, the system success rate starts falling rapidly for the rules that define matrix cracking toward the blade-tip zone and for the rules that define moderate and severe debonding/delamination at the root.

During the analysis of misclassification of the rules [40], the reason for the sudden fall in success rates at higher noise levels is that the GFS is unable to isolate the damage levels due to higher noise in the data. However, it is observed that even at the higher noise levels, the GFS can isolate damage locations accurately.

Implementation of SHM System

The SHM system can be implemented on the helicopter rotor blade for prediction of physical damage and residual life of the blade. The schematic diagram of implementation of the SHM system is shown in Fig. 14. As shown in Fig. 14, for global GFS, tip deflection, and root forces, and for local GFS, the strains measured at five locations can be compared with the database of measurements from the undamaged blade at a given trim condition. Further, using the data-reduction algorithm, the measurement deltas can be calculated and input to the GFS for prediction of the physical damage and residual life of the blade. As shown in Table 1 for global SHM and in Table 2 for local SHM, the maintenance norms can be developed for giving direct instructions to maintenance engineers. This will be more helpful for optimal and safe use of composite rotor blades than the "safe-life" method. Because this method gives intermediate residual-life zones, it will help in reducing the overhauling time.

Conclusions

A numerical method is developed to link the physics-based damage models with phenomenological models to predict the life consumption of the composite rotor blade. Further, an automated online SHM approach is created for prediction of physical damage and life consumption of the composite rotor blade using the simulated measurement deltas obtained by an aeroelastic analysis of the composite rotor blade based on genetic fuzzy systems. The GFS for prediction of global physical damage and life consumption is developed using blade response and load-based measurements. The GFS for prediction of local physical damage and life consumption is developed using the strain-based measurement deltas. The following conclusions are drawn from the study.

1) The total life of the composite rotor blade can be divided into three stages based on the physics-based damage modes such as matrix cracking, debonding/delamination, and fiber breakage. The first stage is dominated by matrix cracking and shows rapid stiffness reduction that consumes 12–15% of the total blade life. The second stage is dominated by debonding/delamination that shows stiffness reduction in an almost linear fashion with respect to life consumption. In this stage, life consumption is about 45–55% of the total life. The third stage is dominated by fiber breakage that leads to the final failure of the composite rotor blade.

2) The success rate of the global GFS depends upon the number of measurements, type of measurements, and noise level in the measurement data.

3) The global GFS developed at a training noise level of 0.15 using displacement-based measurement deltas gives good success rates up

to a noise level of 0.05. The use of load-based measurement deltas in the GFS leads to good performance up to a noise level of 0.1. When both loads and response are used as measurements, the GFS shows good performance up to a noise level of 0.2.

4) The local GFS gives good results up to a noise level of 0.05. For higher noise levels, success rates of the local GFS starts falling drastically, because this system is unable to isolate the damage levels. However, it is observed that the system can isolate damage locations in the matrix-cracking damage zone accurately, even at higher noise levels.

References

[1] Knight, P., Cook, J., and Azzam, H., "Intelligent Management of Helicopter Health and Usage Management Systems Data," *Proceedings of the Institution of Mechanical Engineers, Part G (Journal of Aerospace Engineering)*, Vol. 219, No. G6, 2005, pp. 507–524.

[2] Postdam, M., Yeo, H., and Johnson, W., "Rotor Airloads Prediction Using Loose Aerodynamic/Structural Coupling," *Journal of Aircraft*, Vol. 43, No. 3, 2006, pp. 732–742.

[3] Zhao, Q. J., Xu, G. H., and Zhao, J. G., "New Hybrid Method for Predicting the Flowfields of Helicopter Rotors," *Journal of Aircraft*, Vol. 43, No. 2, 2006, pp. 372–380.

[4] Krzysiak, A., and Narkiewicz, J., "Aerodynamic Loads on Airfoil with Trailing-Edge Flap Pitching with Different Frequencies," *Journal of Aircraft*, Vol. 43, No. 2, 2006, pp. 407–418.

[5] Wang, S. D., Danai, K., and Wilson, M., "Adaptive Method of Helicopter Track and Balance," *Journal of Dynamic Systems, Measurement, and Control*, Vol. 127, No. 2, 2005, pp. 275–282.

[6] Wang, S. D., Danai, K., and Wilson, M., "A Probability-based Approach to Helicopter Rotor Tuning," *Journal of the American Helicopter Society*, Vol. 50, No. 1, 2005, pp. 56–64.

[7] Rosen, A., and BenAri, R., "Mathematical Modelling of a Helicopter Rotor Track and Balance: Theory," *Journal of Sound and Vibration*, Vol. 200, No. 5, 1997, pp. 589–603.

[8] BenAri, R., and Rosen, A., "Mathematical Modelling of a Helicopter Rotor Track and Balance: Results," *Journal of Sound and Vibration*, Vol. 200, No. 5, 1997, pp. 605–620.

[9] Azzam, H., and Andrew, M. J., "The Use of Math-Dynamic Model to Aid the Development of Integrated Health and Usage Monitoring," *Proceedings of the Institution of Mechanical Engineers, Part G (Journal of Aerospace Engineering)*, Vol. 206, No. 1, 1992, pp. 71–76.

[10] Ganguli, R., Chopra, I., and Haas, D. J., "Formulation of a Helicopter Rotor-System Damage Detection Methodology," *Journal of the American Helicopter Society*, Vol. 41, No. 44, Oct. 1996, pp. 302–312.

[11] Ganguli, R., Chopra, I., and Haas, D. J., "Simulation of Helicopter Rotor-System Structural Damage, Blade Mistracking, Friction and Freeplay," *Journal of Aircraft*, Vol. 35, No. 4, July–Aug. 1998, pp. 591–597.

[12] Ganguli, R., "Health Monitoring of Helicopter Rotor in Forward Flight Using Fuzzy Logic," *AIAA Journal*, Vol. 40, No. 12, Dec. 2002, pp. 2773–2781.

[13] Pawar, P. M., and Ganguli, R., "On the Effect of Matrix Cracks in Composite Helicopter Rotor Blade," *Composites Science and Technology*, Vol. 65, Nos. 3–4, Mar. 2005, pp. 581–594.

[14] Pawar, P. M., and Ganguli, R., "Modeling Multi-Layer Matrix Cracking in Thin-Walled Composite Rotor Blade," *Journal of the American Helicopter Society*, Vol. 50, No. 4, Oct. 2005, pp. 354–366.

[15] Pawar, P. M., and Ganguli, R., "Modeling Progressive Damage Accumulation in Thin Walled Composite Beams for Rotor Blade Applications," *Composites Science and Technology*, Vol. 66, No. 13, Oct. 2006, pp. 2337–2349.

[16] Pawar, P. M., and Ganguli, R., "On the Effect of Progressive Damage on Composite Helicopter Rotor System Behavior," *Composite Structures*, Vol. 78, No. 3, 2007, pp. 410–423.

[17] Yang, M., Chopra, I., and Haas, D. J., "Sensitivity of Rotor-Fault-Induced Vibrations to Operational and Design Parameters," *Journal of the American Helicopter Society*, Vol. 49, No. 3, July 2004, pp. 328–339.

[18] Stevens, P. L., "Active Interrogation of Helicopter Main Rotor Faults Using Trailing Edge Flap Actuation," Ph.D. Dissertation, Pennsylvania State Univ., University Park, PA, May 2001.

[19] Lakshmanan, K. A., and Pines, D. J., "Damage Identification of Chordwise Crack Size and Location in Uncoupled Composite Rotorcraft Flexbeams," *Journal of Intelligent Material Systems and Structures*, Vol. 9, No. 2, Feb. 1998, pp. 146–155.

[20] Fatemi, A., and Yang, L., "Cumulative Fatigue Damage and Life Prediction Theories a Survey of the State of the Art for Homogeneous Materials," *International Journal of Fatigue*, Vol. 20, No. 1, Jan. 1998, pp. 9–34.

[21] Degrieck, J., and Van Paepegem, W., "Fatigue Damage Modeling of Fibre-Reinforced Composite Materials Review," *Applied Mechanics Reviews*, Vol. 54, No. 4, July 2001, pp. 279–300.

[22] Nicholas, T., and Russ, S. M., "Elevated Temperature Fatigue Behavior of SCS-6/Ti-24Al-11Nb," *Materials Science and Engineering A*, Vol. 153, Nos. 1–2, May 1992, pp. 514–519.

[23] Subramanian, S., Reifsnider, K. L., and Stinchcomb, W. W., "A Cumulative Damage Model to Predict the Fatigue Life of Composite Laminates Including the Effect of a Fibre-Matrix Interface," *International Journal of Fatigue* Vol. 17, No. 5, 1995, pp. 343–351.

[24] Halverson, H. G., Curtin, W. A., and Reifsnider, K. L., "Fatigue Life of Individual Composite Specimens based on Intrinsic Fatigue Behavior," *International Journal of Fatigue*, Vol. 19, No. 5, May 1997, pp. 369–377.

[25] Mao, H., and Mahadevan, S., "Fatigue Damage Modelling of Composite Materials," *Composite Structures*, Vol. 58, No. 4, Dec. 2002, pp. 405–410.

[26] Moon, T. C., Kim, H. Y., and Hwang, W., "Natural Frequency Reduction Model for Matrix Dominated Fatigue Damage of Composite Laminates," *Composite Structures*, Vol. 62, No. 1, Oct. 2003, pp. 19–26.

[27] Bedewi, N. E., and Kung, D. N., "Effect of Fatigue Loading on the Modal Properties of Composite Structures and its Utilization for Prediction of Residual Life," *Composite Structures* Vol. 37, Nos. 3–4, Mar.–Apr. 1997, pp. 357–371.

[28] Roy, N., and Ganguli, R., "Filter Design Using Radial Basis Function Neural Network and Genetic Algorithm for Improved Operational Health Monitoring," *Applied Soft Computing*, Vol. 6, No. 2, 2006, pp. 154–169.

[29] Roy, N., and Ganguli, R., "Helicopter Rotor Blade Frequency Evolution with Damage Growth and Signal Processing," *Journal of Sound and Vibration*, Vol. 283, Nos. 3–5, 2005, pp. 821–851.

[30] Ganguli, R., Chopra, I., and Haas, D. J., "Detection of Helicopter Rotor System Simulated Faults Using Neural Networks," *Journal of the American Helicopter Society*, Vol. 42, No. 2, Apr. 1997, pp. 161–171.

[31] Reddy, R. R. K., and Ganguli, R., "Structural Damage Detection in a Helicopter Rotor Blade Using Radial Basis Function Neural Networks," *Smart Materials and Structures*, Vol. 12, No. 2, Apr. 2003, pp. 232–241.

[32] Ramanujam, N., Nakamura, T., and Urago, M., "Identification of Embedded Interlaminar Flaw Using Inverse Analysis," *International Journal of Fracture*, Vol. 132, No. 2, Mar. 2005, pp. 153–173.

[33] Iwasaki, A., and Todoroki, A., "Delamination Identification of CFRP Structure by Discriminant Analysis Using Mahalanobis Distance," *Key Engineering Materials*, Vols. 270–273, Nos. 1–3, 2004, pp. 1859–1865.

[34] Rao, M. A., Srinivas, J., and Murthy, B. S. N., "Damage Detection in Vibrating Bodies Using Genetic Algorithms," *Computers and Structures*, Vol. 82, Nos. 11–12, May 2004, 963–968.

[35] Ramu, S. A., and Johnson, V. T., "Damage Assessment of Composite of Composite Structures- A Fuzzy-Logic Integrated Neural Network Approach," *Computers and Structures*, Vol. 57, No. 3, Nov. 1995, pp. 491–502.

[36] Ganguli, R., "A Fuzzy Logic System for Ground Based Structural Health Monitoring of a Helicopter Rotor Using Modal Data," *Journal of Intelligent Material Systems and Structures*, Vol. 12, No. 6, June 2001, pp. 397–407.

[37] Nyongesa, H. O., Otieno, A. W., and Rosin, P. L., "Neural Fuzzy Analysis of Delaminated Composites from Shearography Imaging," *Composite Structures*, Vol. 54, Nos. 2–3, Nov.–Dec. 2001, pp. 313–318.

[38] Alkahe, J., Rand, O., and Oshman, Y., "Helicopter Health Monitoring Using an Adaptive Estimator," *Journal of the American Helicopter Society*, Vol. 48, No. 3, 2003, pp. 199–210.

[39] Pawar, P. M., and Ganguli, R., "Genetic Fuzzy System for Damage Detection in Beams and Helicopter Rotor Blades," *Computer Methods in Applied Mechanics and Engineering*, Vol. 192, Nos. 16–18, Apr. 2003, pp. 2031–2057.

[40] Pawar, P. M., and Ganguli, R., "Matrix Cracking Detection in Thin-Walled Composite Beam Using Genetic Fuzzy System," *Journal of Intelligent Material Systems and Structures*, Vol. 16, No. 5, Mar. 2005, pp. 381–468.

[41] Chandra, R., and Chopra, I., "Structural Response of Composite Beams and Blades with Elastic Couplings," *Composites Engineering*, Vol. 2, Nos. 5–6, 1992, pp. 347–374.

[42] Ganguli, R., and Chopra, I., "Aeroelastic Optimization of a Helicopter Rotor with Two-Cell Composite Blades," *AIAA Journal*, Vol. 34, No. 4, Apr. 1996, pp. 835–841.

[43] Adolfsson, E., and Gudmundson, P., "Thermoelastic Properties in Combined Bending and Extension of Thin Composite Laminates with Transverse Matrix Cracks," *International Journal of Solids and Structures*, Vol. 34, No. 16, June 1997, pp. 2035–2060.

[44] Kosko, B., *Fuzzy Engineering*, Prentice–Hall, Upper Saddle River, NJ, 1997.